Annals of Solid and Structural Mechanics manuscript No.
(will be inserted by the editor)

Numerical study of a thermo-hydro-mechanical damage model for unsaturated porous media

C. Arson · B. Gatmiri

Received: date / Accepted: date

Abstract The "THHMD" damage model presented in this article is dedicated to non-isothermal unsaturated porous media. The proposed frame is based on the use of independent state variables (net stress, suction and thermal stress). The damaged behavior law stems from phenomenological and micro-mechanical concepts. The stress/strain thermodynamic conjugation relations are derived from the free energy, which is written as the sum of damaged elastic deformation energies and of residual strain potentials. The damaged mechanical rigidities are computed by applying the Principle of Equivalent Elastic Energy for each stress state variable. The influence of damage on liquid water and vapor transfers is accounted for by introducing internal length parameters, related to specific damage-induced intrinsic conductivities. Damage is assumed to have an isotropic influence on air and heat flows, through the inelastic component of volumetric strains. The "THHMD" model has been implemented in Θ-Stock Finite Element code. The mechanical aspects of the model have been validated. A full scale thermo-hydro-mechanical engineering problem has been reproduced. The elastic predictions are in satisfactory agreement with the reference results, and the damaged behavior of the unsaturated massif shows good trends.

Keywords Continuum Damage Mechanics · unsaturated porous media · independent state variables · thermodynamics · micro-mechanics · transfer rules · Finite Element Method · nuclear waste repository

C. Arson
University of Paris-Est (France), UR Navier (CERMES), ENPC
Tel.: +33 1 64 15 35 24
Fax: +33 1 64 15 35 62
E-mail: arson@cermes.enpc.fr
Present address:
CERMES, Ecole Nationale des Ponts et Chaussées
6-8 av. Blaise Pascal
Cité Descartes, Champs-sur-Marne
77455 Marne-la-Vallé cedex 2
FRANCE

B. Gatmiri
Agence Nationale pour la gestion des Dchets RAdioactifs (ANDRA), FRANCE
E-mail: behrouz.gatmiri@andra.fr

1 Introduction

Damage modeling has become a crux point in the study of the Excavation Damaged Zone (EDZ) [28], [29]. In the context of nuclear waste storage, cracking effects have to be accounted for in the constitutive laws of non-isothermal unsaturated porous media [21]. The two main stakes are the introduction of damage in the behavior law of an unsaturated porous medium in the one hand, and the modeling of fluid and heat transfers in a cracked porous medium in the other hand. Most of the past studies separate both problems, presenting either flow models in fracture networks, or hydro-mechanical continuum damage models [3].
Micro-mechanical damage models aim at representing the effect of damage occurring at the microscopic scale on the behavior of the material at the macroscopic scale, or at least, at the meso-scale of the Representative Elementary Volume (REV). Damage is microscopically generated by nucleation or micro-void coalescence. This induces a loss of effective surface in the material [23]. Stresses are reoriented, which gives a damage-induced anisotropy to the material. Most of the authors model these phenomena by defining an effective stress, as the stress that develops in the fictive undamaged counterpart of the system [7]. Although microscopic, damage is non-local, which requires the introduction of internal length parameters [6]. *Phenomenological damage models* are based on postulated expressions of thermodynamic potentials [32]. The frame is more abstract than in micro-mechanical theories, but the thermodynamic consistency of the formulation is often easier to establish.
The main differences between flow models lie in the number of represented continua, and in the modeling of fluid exchanges between continua. In *multimodal models*, the pores of the intact matrix and the cracks generated by damage growth communicate, and form a unique porous network. Only one balance equation is necessary to model the flow of a fluid among the REV. However, the relative organization of porous heterogeneity makes it impossible to express the global hydraulic properties of the REV by a mere retention curve [15]. In *multi-continua models*, several porous networks drive the flow and behave as separate entities. A fractured porous material is frequently modeled as a dual continuum, with the pores of the intact matrix on the one hand, and the crack network on the other hand. For a given pore fluid, there is one balance equation per continuum, each of which being characterized by its retention properties. In multi-porosity models [39], one continuum is generally assumed to dominate in driving the flow, and its permeability is considered equal to the permeability of the REV. In multi-permeability models [34], one permeability is defined for each network, and a homogenization is necessary in order to get the permeability of the REV.
In the following, it will be understated that the solid phase of the Representative Elementary Volume is relative to the solid skeleton, the liquid phase, to pore liquid water, and the gaseous phase, to a mixture of gaseous air and vapor. In Section 2, the "HHMD" model (hydro-mechanical damage model for unsaturated porous media), previously developed by the authors to study the effects of cracking in an unsaturated porous medium [2], [4], has been extended to non-isothermal conditions. The principal development stages of this new "THHMD" (thermo-hydro-mechanical damage model for unsaturated porous media) model are explained, both for the behavior law and the transfer rules. In Section 3, numerical validation tests performed on dry and saturated geomaterials are presented. A more complex numerical application, simulating a full scale nuclear waste repository, is studied in Section 4.

2 Brief statement of the theoretical framework of the model

2.1 Choice of the stress and damage variables

The "THHMD" model is part of Continuum Damage Mechanics (CDM). It is based on both phenomenological and micro-mechanical principles. Damage is considered as a dissipative effect, originating elastic energy losses. In three dimensions, such a representation of damage should require a fourth-order tensor, but using the second-order crack density tensor gives a very satisfactory approximation of the energetic process [26]. The damage variable $\mathbf{\Omega}$ has thus been chosen as the homogenized crack density tensor. It is expressed in a fixed principal base as:

$$\mathbf{\Omega} := \sum_{I=1}^{3} d^I \mathbf{n^I} \otimes \mathbf{n^I} \tag{1}$$

Conceptually, the Representative Elementary Volume is damaged by three meso-cracks, representing three families of approximately parallel micro-cracks. If V is the volume of the REV, the volume occupied by the I^{th} meso-crack in the REV equals $V\, d^I$. $\mathbf{n^I}$ eigenvector is the vector which is normal to the I^{th} crack plane.

Most of the existing damage models dedicated to unsaturated porous media are formulated by means of an effective stress, defined in the same way as Bishop's stress [3]. These framework are not satisfactory to represent some aspects of the behavior of unsaturated soils, like "wetting collapse" [16], [25]. On the contrary, the proposed damage model is formulated in independent state variables. In isothermal conditions, the stress state variables are net stress $\boldsymbol{\sigma}" = \boldsymbol{\sigma} - p_a \boldsymbol{\delta}$ and suction $s = p_a - p_w$, in which $\boldsymbol{\sigma}$ is the total stress tensor, and $\boldsymbol{\delta}$, the second-order identity tensor. p_w and p_a are respectively the pore pressure of the wetting phase (liquid water in the following) and the pore pressure of the non-wetting phase (gaseous air in the following). The model is presently extended to thermal effects by using an additional stress state variable. Temperature is assumed to have isotropic effects on strains [19], which results in the use of a scalar thermal stress p_T.

Following the same approach as Gatmiri [17], [18], [20], the total strain tensor is split in independent strain state variables, each of which being conjugate to one independent stress state variable [4]. Consequently, the following pairs of state variables are used:

$$\begin{cases} \boldsymbol{\sigma}" & \leftrightarrow & \boldsymbol{\epsilon}_{\mathbf{M}} \\ s & \leftrightarrow & \epsilon_{Sv} \\ p_T & \leftrightarrow & \epsilon_{Tv} \end{cases} \tag{2}$$

$\boldsymbol{\epsilon}_{\mathbf{M}}$, ϵ_{Sv} and ϵ_{Tv} are respectively the mechanical strain tensor, the capillary volumetric strain and the thermal volumetric strain. The adopted state variables being independent, the incremental total strain tensor $d\boldsymbol{\epsilon}$ may be written as:

$$d\boldsymbol{\epsilon} = d\boldsymbol{\epsilon}^{\mathbf{e}}_{\mathbf{M}} + d\boldsymbol{\epsilon}^{\mathbf{d}}_{\mathbf{M}} + \frac{1}{3}\boldsymbol{\delta} d\epsilon^e_{Sv} + \frac{1}{3}\boldsymbol{\delta} d\epsilon^d_{Sv} + \frac{1}{3}\boldsymbol{\delta} d\epsilon^e_{Tv} + \frac{1}{3}\boldsymbol{\delta} d\epsilon^d_{Tv} \tag{3}$$

"e" and "d" subscripts refer to the elastic and inelastic (damaged) strain components, respectively.

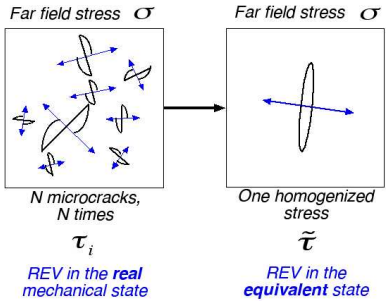

Fig. 1 Equivalent mechanical state in a 2D damaged REV.

2.2 Thermodynamic aspects of the behavior law formulation

2.2.1 Inequality of Clausius-Duhem

Let's consider the Representative Elementary Volume as an open thermodynamic system. Assuming that the solid grains constituting the skeleton are incompressible, the Inequality of Clausius-Duhem (ICD) may be expressed in terms of three state variables instead of four [11], [12]. The ICD then depends on total stress, suction and temperature [25]:

$$\sigma" \, \Delta\epsilon \, + s\Delta \left(-nS_w\right) \, - \eta\Delta T \, - \Delta\Psi_s \left(\epsilon, nS_w, T, \mathbf{\Omega}\right) \geq 0 \tag{4}$$

in which η is entropy. With the state variables adopted in the "THHMD" model, the ICD may be rewritten as [4]:

$$\boldsymbol{\sigma}" \, : \, \Delta\boldsymbol{\epsilon}_{\mathbf{M}} \, + s \, \Delta\epsilon_{Sv} \, + p_T \, \Delta\epsilon_{Tv} \, - \Delta\Psi_s \left(\boldsymbol{\epsilon}_{\mathbf{M}}, \epsilon_{Sv}, \epsilon_{Tv}, \mathbf{\Omega}\right) \geq 0 \tag{5}$$

in which Ψ_s is Helmholtz free energy.

2.2.2 Equivalent mechanical state

In the *real mechanical state*, N micro-cracks are assumed to open in the REV under the influence of N corresponding micro-stresses, noted $\boldsymbol{\tau_i}$. Following the approach of Swoboda and Yang [37], it is assumed that an isothermal dry damaged material may be represented in an *equivalent mechanical state*, in which the material may be considered intact and submitted to an equivalent crack-related meso-stress $\widetilde{\boldsymbol{\tau}}$:

$$\widetilde{\boldsymbol{\tau}} := \sum_{i=1}^{N} \boldsymbol{\tau_i} \tag{6}$$

The stress $\widetilde{\boldsymbol{\sigma}}$, applied to the isothermal dry REV in the equivalent mechanical state, is the sum of the real far field stress $\boldsymbol{\sigma}$ and the equivalent crack-related stress $\widetilde{\boldsymbol{\tau}}$ (See Figure 1):

$$\widetilde{\boldsymbol{\sigma}} \, = \, \boldsymbol{\sigma} \, + \, \widetilde{\boldsymbol{\tau}} \tag{7}$$

For a dry and isothermal material, the equivalent stress $\widetilde{\boldsymbol{\sigma}}$ is thermodynamically conjugate to the equivalent total strains by a damaged elastic potential $\Psi_e \left(\widetilde{\boldsymbol{\epsilon}}, \mathbf{\Omega}\right)$, whereas

the real stress $\boldsymbol{\sigma}$ is conjugate to real strains by Helmholtz free energy $\Psi_s\left(\boldsymbol{\epsilon}, \boldsymbol{\Omega}\right)$. It is assumed that the real and equivalent strain tensors are equal, and that the equivalent damaged mechanical rigidity equals the real rigidity, damaged by the equivalent damage tensor: $\widetilde{\mathbf{D_e}}\left(\boldsymbol{\Omega}\right) = \mathbf{D_e}\left(\widetilde{\boldsymbol{\Omega}}\right)$. Being homogenized, the damage variable used in the "THHMD" model is the same in the equivalent and in the real mechanical states, and thus: $\widetilde{\mathbf{D_e}}\left(\boldsymbol{\Omega}\right) = \mathbf{D_e}\left(\boldsymbol{\Omega}\right)$. Consequently, the following conjugation relations apply to the isothermal dry porous medium:

$$\begin{cases} \Psi_s^*(\boldsymbol{\sigma}, \boldsymbol{\Omega}) + \Psi_s(\boldsymbol{\epsilon}, \boldsymbol{\Omega}) \,=\, \boldsymbol{\sigma} \,:\, \boldsymbol{\epsilon} \\ \boldsymbol{\epsilon} \,=\, \frac{\partial \Psi_s^*(\boldsymbol{\sigma}, \boldsymbol{\Omega})}{\partial \boldsymbol{\sigma}}, \quad \boldsymbol{\sigma} \,=\, \frac{\partial \Psi_s(\boldsymbol{\epsilon}, \boldsymbol{\Omega})}{\partial \boldsymbol{\epsilon}} \end{cases} \tag{8}$$

$$\begin{cases} \Psi_e^*(\widetilde{\boldsymbol{\sigma}}, \boldsymbol{\Omega}) + \Psi_e(\boldsymbol{\epsilon}, \boldsymbol{\Omega}) \,=\, \widetilde{\boldsymbol{\sigma}} \,:\, \boldsymbol{\epsilon} \\ \boldsymbol{\epsilon} \,=\, \frac{\partial \Psi_e^*(\widetilde{\boldsymbol{\sigma}}, \boldsymbol{\Omega})}{\partial \widetilde{\boldsymbol{\sigma}}}, \quad \widetilde{\boldsymbol{\sigma}} \,=\, \frac{\partial \Psi_e(\boldsymbol{\epsilon}, \boldsymbol{\Omega})}{\partial \boldsymbol{\epsilon}} \end{cases} \tag{9}$$

$*$ subscript refers to the partial Legendre transform of the thermodynamic potentials at stake. An energetic potential is always defined more or less a constant. After combining equations 7, 8 and 9, and after integration, Helmholtz free energy turns to be expressed as:

$$\Psi_s(\boldsymbol{\epsilon}, \boldsymbol{\Omega}) \,=\, \Psi_e(\boldsymbol{\epsilon}, \boldsymbol{\Omega}) \,-\, \widetilde{\boldsymbol{\tau}} \,:\, \boldsymbol{\epsilon} \tag{10}$$

It may easily be assumed that the crack-related meso-stress is parallel to the damage tensor [37]:

$$\widetilde{\boldsymbol{\tau}} \,=\, g\, \boldsymbol{\Omega} \tag{11}$$

g is a rigidity-like scalar. Introducing relation 11 into equation 10 provides an expression of the free energy which is similar to the one used by Dragon and Halm [13].

2.2.3 Expression of Helmholtz free energy

Adapting the concept of equivalent mechanical state to non isothermal unsaturated porous media, Helmholtz free energy is finally assumed to take the following form:

$$\begin{aligned} &\Psi_s(\boldsymbol{\epsilon}_{\mathbf{M}}, \epsilon_{Sv}, \epsilon_{Tv}, \boldsymbol{\Omega}) \,:=\, \Psi_e(\boldsymbol{\epsilon}_{\mathbf{M}}, \epsilon_{Sv}, \epsilon_{Tv}, \boldsymbol{\Omega}) \\ &-g_M\, \boldsymbol{\Omega} \,:\, \boldsymbol{\epsilon}_{\mathbf{M}} \,-\, \tfrac{g_S}{3}\, \boldsymbol{\Omega} \,:\, \boldsymbol{\delta}\, \epsilon_{Sv} \,-\, \tfrac{g_T}{3}\, \boldsymbol{\Omega} \,:\, \boldsymbol{\delta}\, \epsilon_{Tv} \end{aligned} \tag{12}$$

The degraded elastic energy $\Psi_e(\boldsymbol{\epsilon}_{\mathbf{M}}, \epsilon_{Sv}, \epsilon_{Tv}, \boldsymbol{\Omega})$ is written as the sum of three damaged elastic energies, each of which being related to an independent state variable:

$$\Psi_e(\boldsymbol{\epsilon}_{\mathbf{M}}, \epsilon_{Sv}, \epsilon_{Tv}, \boldsymbol{\Omega}) \,:=\, \frac{1}{2}\boldsymbol{\epsilon}_{\mathbf{M}} \,:\, \mathbf{D_e}\left(\boldsymbol{\Omega}\right) \,:\, \boldsymbol{\epsilon}_{\mathbf{M}} \,+\, \frac{1}{2}\epsilon_{Sv}\beta_s\left(\boldsymbol{\Omega}\right)\epsilon_{Sv} \,+\, \frac{1}{2}\epsilon_{Tv}\beta_T\left(\boldsymbol{\Omega}\right)\epsilon_{Tv} \tag{13}$$

$\mathbf{D_e}\left(\boldsymbol{\Omega}\right)$, $\beta_s\left(\boldsymbol{\Omega}\right)$ and $\beta_T\left(\boldsymbol{\Omega}\right)$ are the damaged mechanical, capillary and thermal rigidities respectively. Their explicit expressions will be computed in the following subsection,

by a micro-mechanical approach. Using the ICD 5 provides the stress/strain conjugation relations, which are derived from the expression of the free energy (equations 12 and 13).

$$\begin{cases} \boldsymbol{\sigma}\text{"} = \mathbf{D_e}\left(\boldsymbol{\Omega}\right) : \boldsymbol{\epsilon_M} - g_M\,\boldsymbol{\Omega} \\ s = \beta_s\left(\boldsymbol{\Omega}\right)\epsilon_{Sv} - \frac{g_S}{3}\,\boldsymbol{\delta} : \boldsymbol{\Omega} \\ p_T = \beta_T\left(\boldsymbol{\Omega}\right)\epsilon_{Tv} - \frac{g_T}{3}\,\boldsymbol{\delta} : \boldsymbol{\Omega} \\ \mathbf{Y_d} = -\frac{1}{2}\boldsymbol{\epsilon_M} : \frac{\partial \mathbf{D_e}(\boldsymbol{\Omega})}{\partial \boldsymbol{\Omega}} : \boldsymbol{\epsilon_M} - \frac{1}{2}\epsilon_{Sv}\frac{\partial \beta_s(\boldsymbol{\Omega})}{\partial \boldsymbol{\Omega}}\epsilon_{Sv} - \frac{1}{2}\epsilon_{Tv}\frac{\partial \beta_T(\boldsymbol{\Omega})}{\partial \boldsymbol{\Omega}}\epsilon_{Tv} \\ +g_M\,\boldsymbol{\epsilon_M} + \frac{g_S}{3}\epsilon_{Sv}\boldsymbol{\delta} + \frac{g_T}{3}\epsilon_{Tv}\boldsymbol{\delta} \end{cases} \tag{14}$$

$\mathbf{Y_d}$ is the damage-conjugate stress. In absence of deformation, the stress state variables are non zero. These residual values depend on cumulated damage: $\boldsymbol{\sigma}\text{"} = -g_M\,\boldsymbol{\Omega}$, $s = -\frac{g_S}{3}\,\boldsymbol{\delta} : \boldsymbol{\Omega}$, $p_T = -\frac{g_T}{3}\,\boldsymbol{\delta} : \boldsymbol{\Omega}$. Physically, the material has to be submitted to residual compressions in order to go back to its non-deformed state after unloading. In other words, after a mere unloading (null stress state variables), a residual traction remains, which generates residual strains. The introduction of crack-related rigidities g_M, g_S and g_T thus enables the representation of residual strains after unloading, without requiring to additional plastic potentials.

2.3 Micromechanical aspects of the behavior law formulation

A micro-mechanical approach is used to compute the damage rigidities $\mathbf{D_e}\left(\boldsymbol{\Omega}\right)$, $\beta_s\left(\boldsymbol{\Omega}\right)$ and $\beta_T\left(\boldsymbol{\Omega}\right)$. The concept of effective stress, commonly used in Continuum Damage Mechanics [23], [27], is extended to the three stress state variables used in the "THHMD" model. Applying the operator of Cordebois and Sidoroff [10] to the three "THHMD" stress state variables results in:

$$\begin{cases} \widehat{\boldsymbol{\sigma}\text{"}} := \left(\boldsymbol{\delta} - \boldsymbol{\Omega}\right)^{-1/2} \cdot \boldsymbol{\sigma}\text{"} \cdot \left(\boldsymbol{\delta} - \boldsymbol{\Omega}\right)^{-1/2} \\ \widehat{s} := \frac{s}{3}\left(\boldsymbol{\delta} - \boldsymbol{\Omega}\right)^{-1} : \boldsymbol{\delta} \\ \widehat{p_T} := \frac{p_T}{3}\left(\boldsymbol{\delta} - \boldsymbol{\Omega}\right)^{-1} : \boldsymbol{\delta} \end{cases} \tag{15}$$

The damaged rigidities are determined by application of the Principle of Equivalent Elastic Energy (PEEE). The final expressions are [4]:

$$\begin{cases} \mathbf{D_e}\left(\boldsymbol{\Omega}\right) = \mathbf{M}\left(\boldsymbol{\Omega}\right)^{-1} : \mathbf{D_e^0} : \mathbf{M}\left(\boldsymbol{\Omega}\right)^{T} \\ \beta_s\left(\boldsymbol{\Omega}\right) = \frac{9\beta_s^0}{\left[\left(\boldsymbol{\delta}-\boldsymbol{\Omega}\right)^{-1} : \boldsymbol{\delta}\right]^2} \\ \beta_T\left(\boldsymbol{\Omega}\right) = \frac{9\beta_T^0}{\left[\left(\boldsymbol{\delta}-\boldsymbol{\Omega}\right)^{-1} : \boldsymbol{\delta}\right]^2} \end{cases} \tag{16}$$

Equations 14 and 16 make it possible to get the complete incremental behavior law. The only remaining unknown at this stage is the increment of damage, which is computed by an associate flow rule depending on tensile strains [4]. The damage yield function f_d is chosen to be homogeneous of degree one in $\mathbf{Y_d}$, which ensures the convexity of the elastic domain [9].

2.4 Damaged transfer rules

Like in the preceding works of Gatmiri [17], [18], [19], [20], liquid water flow is assumed to be diffusive, and to obey an extended Darcy law of the form:

$$\mathbf{V_w} \;=\; -\frac{\Psi_R\left(\theta_w\right)}{\sigma(T_{ref})}\,\frac{d\sigma(T)}{dT}\,\mathbf{K_w}\cdot\boldsymbol{\nabla}\left(T\right) \;+\; \frac{1}{\gamma_w}\,\frac{\sigma(T)}{\sigma(T_{ref})}\,\mathbf{K_w}\cdot\boldsymbol{\nabla}\left(s\right) \;-\; \mathbf{K_w}\cdot\boldsymbol{\nabla}\left(z\right) \quad (17)$$

$\mathbf{V_w}$ is the liquid water velocity (in m.s^{-1}) relatively to the solid skeleton. $\mathbf{K_w}$ is the permeability tensor related to liquid water (in m.s^{-1}), and γ_w is the specific weight of liquid water in standard conditions of temperature and pressure. $\sigma(T)$ is the superficial energy of pore water. The relative capillary potential Ψ_R is defined as [31]: $\Psi_R(\theta_w) = (p_w - p_a)/\gamma_w$, in which θ_w is water content. The influence of cracking on the velocity and on the orientation of liquid flow is taken into account through the intrinsic permeability tensor $\mathbf{K_{int}}$ [4]:

$$\mathbf{K_w} \;=\; k_T(T)\,k_r(S_w)\,\mathbf{K_{int}}\left(n,\boldsymbol{\Omega}\right) \quad (18)$$

In addition to the intrinsic permeability of intact porous media modeled by Gatmiri [17], [18], [19], [20], $\mathbf{K_{int}}$ encompasses a specific crack-related component $\mathbf{k_2}\left(\boldsymbol{\Omega}\right)$, which is computed by assuming that the liquid water flow in micro-carcks is laminar, and that it can be homogenized at the scale of the Representative elementary Volume [4]. Assuming that the meso-cracks damaging the REV are penny-shaped and that their openings are related to their radii by a linear dilatancy rule of coefficient χ [35]:

$$\mathbf{k_2}\left(\boldsymbol{\Omega}\right) \;=\; \frac{\pi^{-2/3}\,\gamma_w}{12\,\mu_w\left(T_{ref}\right)}\,\chi^{4/3}\,b^2\,\sum_{I=1}^{3}\left(d^I\right)^{5/3}\,\left(\boldsymbol{\delta}-\mathbf{n^I}\otimes\mathbf{n^I}\right) \quad (19)$$

In formula 19, b plays the role of an internal length parameter, which is specific to the liquid flow problem. It may be computed if the value of the damaged intrinsic permeability is assessed at a given rate of damage. For example, if K_{wdg}^{max} is the maximal mean value of $\mathbf{k_2}\left(\boldsymbol{\Omega}\right)$, obtained for an isotropic damage state of 95 percent:

$$b \;=\; \frac{\sqrt{6}}{0,95^{5/6}}\,\left(\frac{\pi}{\chi^2}\right)^{1/3}\,\left(\frac{\mu_w\left(T_{ref}\right)}{\gamma_w}\right)^{1/2}\,\left(K_{wdg}^{max}\right)^{1/2} \quad (20)$$

By extension, the limiting value K_{wdg}^{max} is used as an internal length parameter in the "THHMD" model. Damage is a homogenized variable. The porous network constituted by the pores of the intact matrix and by microcracks is thus considered as a unique, connected and unimodal flow network.

Using the same hypotheses and notations as Gatmiri [17], [18], [19], [20], and assuming that vapor transfers are mainly diffusive, the final expression of the vapor flow velocity may be written as:

$$\mathbf{V^*_{vap}} \;=\; \frac{\rho_{vap}}{\rho_w}\,\mathbf{V_{vap}} \;=\; -D_{T_{vap}}\,\boldsymbol{\nabla}\left(T\right) \;+\; D_{P_{vap}}\,\boldsymbol{\nabla}\left(s\right) \quad (21)$$

in which $D_{T_{vap}}$ and $D_{P_{vap}}$ are the thermal and capillary diffusivities of vapor, respectively. Both of them depend on an intrinsic component $D_{int,\,vap}$. It is assumed that cracking accelerates vapor transfers in such a way that the flow formulas used for the

intact porous medium become invalid. As for the modeling of water transfers, vapor intrinsic conductivity $D_{int,\,vap}$ is split into two parts:

$$D_{int,\,vap} := D_{int,\,vap_1}\left(n, s, T, \mathbf{\Omega}\right) + D_{int,\,vap_2}\left(\mathbf{\Omega}\right) \tag{22}$$

$D_{int,\,vap_1}\left(n, s, T, \mathbf{\Omega}\right)$ is a conductivity representing the contribution of the pores of the matrix in the elastic deformation domain. $D_{int,\,vap_2}\left(\mathbf{\Omega}\right)$ represents the contribution of the micro-crack network. It is assumed that vapor goes much faster than liquid water, and that consequently, the fracture network hardly affects the orientation of vapor flow. That is why the damaged component of vapor intrinsic conductivity is expressed as a function of the mean damaged intrinsic conductivity of liquid water $\mathbf{k_2}\left(\mathbf{\Omega}\right)$:

$$D_{int,\,vap_2}\left(\mathbf{\Omega}\right) = \frac{b^*}{3}\,\boldsymbol{\delta} : \mathbf{k_2^*}\left(\mathbf{\Omega}\right) \tag{23}$$

in which the damaged intrinsic conductivity of liquid water is expressed with the vapor transfer internal length b^* instead of b (equation 19). As for the liquid water flow model, b^* may be evaluated if the damaged intrinsic conductivity of vapor is known for a given state of damage.

Air flow is assumed to be diffusive. The expression of air velocity depends on a scalar permeability, which is a function of the void ratio [4], [19]. This latter reflects the influence of total volumetric strains, which encompass a non-elastic component. This non-elastic volumetric strain translates the effect of damage on air transfers. This influence is thus isotropic.

Like in the preceding models of Gatmiri [17], [18], [19], [20], heat transfer is assumed to be governed by diffusion, evaporation and convection. Convection and evaporation are pure fluid phenomena. Therefore, only the diffusive part of heat transfer is likely to be influenced by the degradation of the solid matrix. As for air flow, the heat flow equation of intact porous media is extended to damaged media, and damage is taken into account indirectly and isotropically, through the dependence of the diffusive conductivity to volumetric strains [5].

3 Validation tests on dry and saturated geomaterials

A specific algorithm has been written in order to implement the "THHMD" model in Θ-Stock Finite Element code [19], which has been used to perform the simulations presented in this article.

3.1 Mechanical identification tests

Mechanical laboratory tests have been simulated on Vienne granite (Tab.1) by using the parameters identified by Halm and Dragon [22]. The numerical results are compared to experimental data provided by Homand et al. [24]. In the numerical model, the tested material is assumed to be dry, so that the pore pressure degrees of freedom are neutralized.

Table 1 Mechanical parameters of Vienne granite [22].

E	ν	g_M	g_S	g_T
$8.01 * 10^{10}\, Pa$	0.28	$-3.3 * 10^{8}\, Pa$	0	0

Table 2 Main material parameters of Fontainebleau sandstone [14] [36].

E	ν	g_M	g_S	g_T	k_{w0}	K_{wdg}^{max}
$4.55 * 10^{10}\, Pa$	0.3	$-1.1 * 10^{8}\, Pa$	0	0	$3.33 * 10^{-5}\, m.s^{-1}$	$3.33 * 10^{-3}\, m.s^{-1}$

Triaxial compression tests are reproduced for various confining pressures. A lateral extension test is also simulated. In this latter simulation, the sample is first submitted to an isotropic stress $p_c = 60\, MPa$. The lateral confining pressure p_c is then maintained while the axial stress is increased up the compression limit (amounting to 127 MPa). Last, the lateral confining pressure p_c is progressively decreased to zero while the axial stress is maintained at 127 MPa.
Numerical results and experimental data match very well (Fig. 2). In triaxial compression tests, the initiation of damage occurs when the deviatoric stress reaches 127 MPa, which corresponds exactly to the experimental value of the compression limit [24]. In the lateral extension test, releasing the confining pressure acts as a traction. Tensile strains $\left(\epsilon^{+}\right)$ are thus applied in both lateral directions $\left(\epsilon_{rr}^{+},\, \epsilon_{\theta\theta}^{+}\right)$. In the triaxial compression tests, the sample undergoes tensile strains which are orthogonal to the applied compression. As a result, lateral tensile strains also develop during triaxial compression tests. Damage is assumed to grow with tensile strains. Consequently, in all tests, the axial component of damage is expected to be null ($\Omega_{zz} = 0$), while both lateral damage components are expected to be equal and non zero for a sufficient deviatoric stress ($\Omega_{rr} = \Omega_{\theta\theta} \neq 0$). The numerical results are in agreement with these predictions, for all tests. All the results are not provided in this article. The evolution of the damage components are given for the lateral extension test (Fig.3.a). The radial component of damage is represented for each triaxial compression test on Fig.3.b. As expected, lateral damage grows with the applied deviatoric stress.

3.2 Compression tests on a saturated geomaterial

Some triaxial compression tests performed on saturated Fontainebleau sandstone by Sulem and Ouffroukh [36] have been simulated in undrained and drained conditions. The mechanical parameters identified by Dragon et al. [14] have been used. The intact intrinsic water permeability k_{w0} is taken from the experimental study of Sulem and Ouffroukh [36], for a porosity of 0.21. It is assumed that for a critical isotropic damage state of 95 percent, the damaged water permeability cannot exceed 100 times the intact intrinsic permeability k_{w0}, which results in $K_{wdg}^{max} = 100\, k_{w0}$. The main parameters of Fontainebleau sandstone are given in Tab.2. More details on the choice of the parameters which are required to perform the numerical simulations can be found in [1].

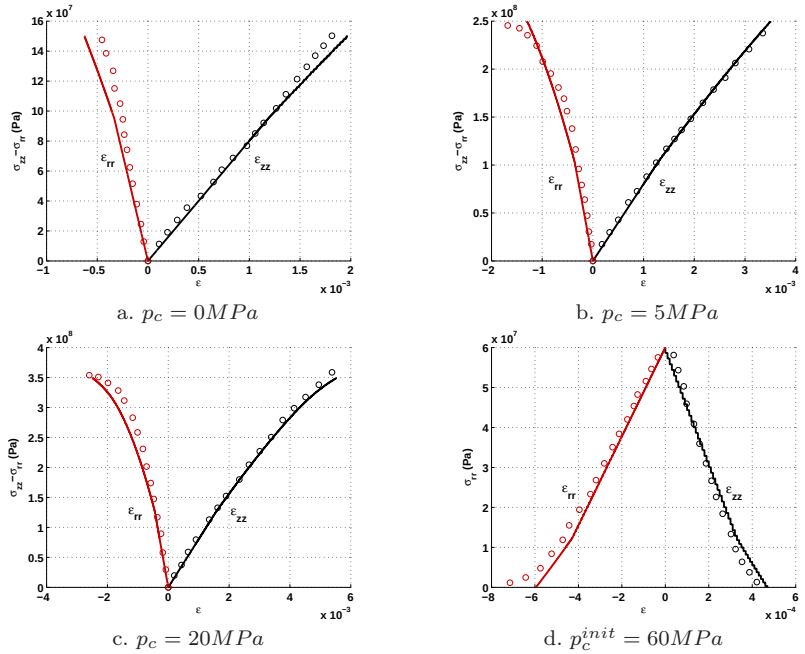

a. $p_c = 0MPa$ b. $p_c = 5MPa$

c. $p_c = 20MPa$ d. $p_c^{init} = 60MPa$

Fig. 2 Triaxial compression tests (a,b,c) and lateral extension test (d) performed on dry granite. Dots: experimental data [24]. Solid lines: numerical results.

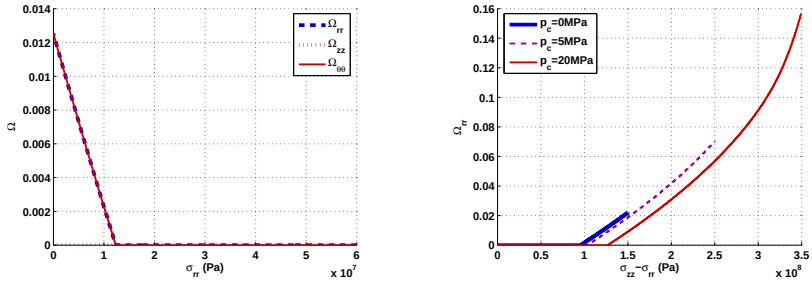

a. b.

Fig. 3 Evolution of damage during the mechanical tests performed on dry granite. a. Lateral extension test. b. Triaxial compression tests.

As can be seen on Fig.4, the deformations and pore pressures computed numerically in undrained conditions are in satisfactory agreement with the experimental data taken from [36] for all the tested confining pressures ($p_c = 28MPa$, $p_c = 40MPa$, $p_c = 50MPa$). Water pore pressure acts as an additional confining pressure. Tensile strains thus develop in the same way as they do during a triaxial compression test performed on a dry material. As a consequence, for a certain rate of deviatoric stress, damage is expected to develop equally in both lateral directions, while keeping null in the axial direction: ($\Omega_{rr} = \Omega_{\theta\theta} \neq 0, \quad \Omega_{zz} = 0$). This phenomenon is well-reproduced in the simulations (Fig. 4.c,f,i).

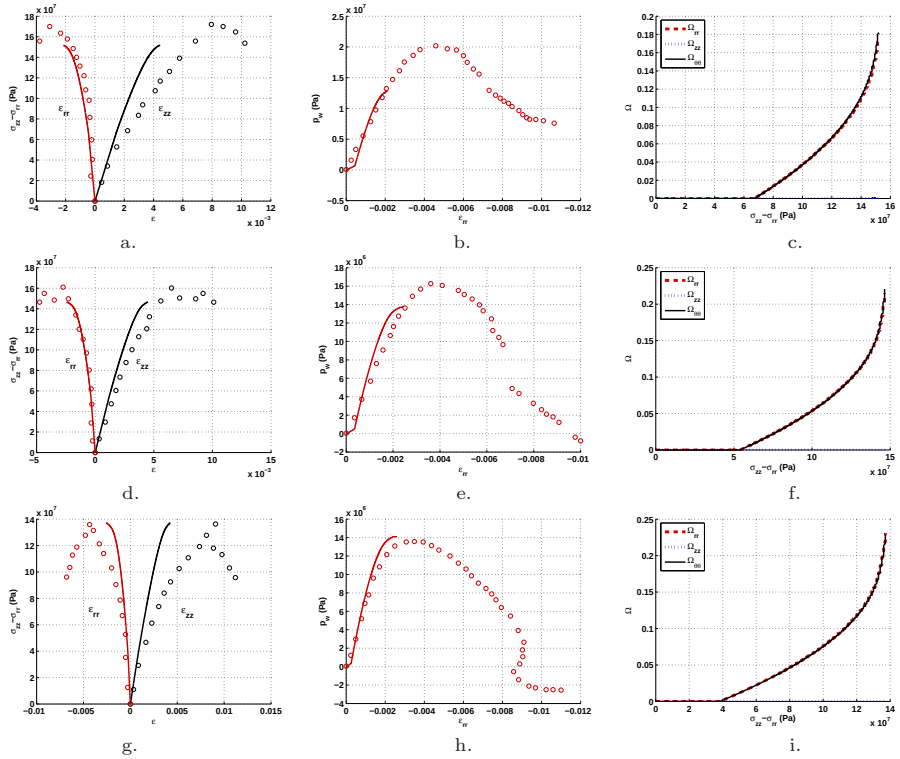

Fig. 4 Undrained triaxial compression tests performed on saturated Fontainebleau sandstone. Dots: experimental data [36]. Solid lines: numerical results. (a,b,c) $p_c = 50\,MPa$. (d,e,f) $p_c = 40\,MPa$. (g,h,i) $p_c = 28\,MPa$.

The deformations obtained with the same confining pressures in drained conditions match the experimental measurements provided by Sulem and Ouffroukh [36] (Fig.5.a,c,e). Contrary to the triaxial compression tests performed on dry granite, simulated drained tests involve water pore pressure degree of freedom. The loading velocity is chosen in order to maintain the value of total stress two order of magnitude higher than the value of water pore pressure. Therefore, drained tests are numerically equivalent to compression tests performed on a dry material. That is why damage trends are the same in both cases (Fig. 3.b and 5.b,d,f).

The damaged water permeability model (equation 19) assumes that the permeability tensor is mainly affected by damage in the directions which belong to a principal meso-crack plane. In other words, the permeability tensor is degraded in the directions which are orthogonal to damage eigenvectors $\mathbf{n^I}$. In drained compression tests, axial damage remains zero whereas both lateral components of the damage tensor develop equally ($\Omega_{rr} = \Omega_{\theta\theta} \neq 0, \quad \Omega_{zz} = 0$). As a result, axial permeability K_{wzz} increases due to the contributions of two components of damage (Ω_{rr} and $\Omega_{\theta\theta}$) whereas lateral permeability components K_{wrr} and $K_{w\theta\theta}$ are affected by only one damage component ($\Omega_{\theta\theta}$ and Ω_{rr} respectively). The evolution of the permeability tensor is shown for the drained triaxial compression test with a confining pressure of 28 MPa (Fig. 6). As expected, all

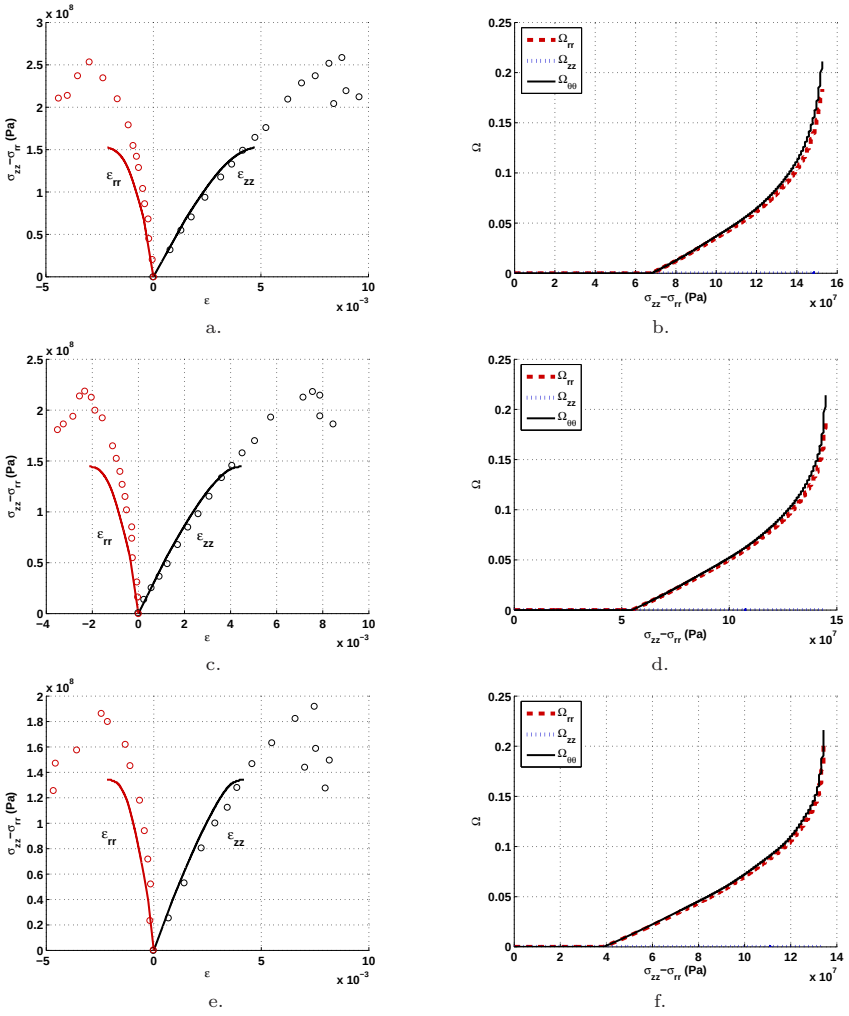

Fig. 5 Drained triaxial compression tests performed on saturated Fontainebleau sandstone. Dots: experimental data [36]. Solid lines: numerical results. (a,b) $p_c = 50\,MPa$. (c,d) $p_c = 40\,MPa$. (e,f) $p_c = 28\,MPa$.

components of permeability are affected by damage, and permeability increases mostly in the axial direction. Due to hydro-mechanical couplings, the reduction of the void ratio measured in the non damaged matrix has also an influence on the final permeability of the medium. That is the reason why K_{wzz} is not exactly equal to $2\,K_{wrr}$. However, the general statement $K_{wrr} = K_{w\theta\theta} < K_{wzz}$ is verified.

3.3 Mechanical validation with the elastic theory of tunnels

Gallery excavations are often modeled as a mechanical unloading at the tunnel wall. The problem has been solved numerically for a dry massif submitted to an initial

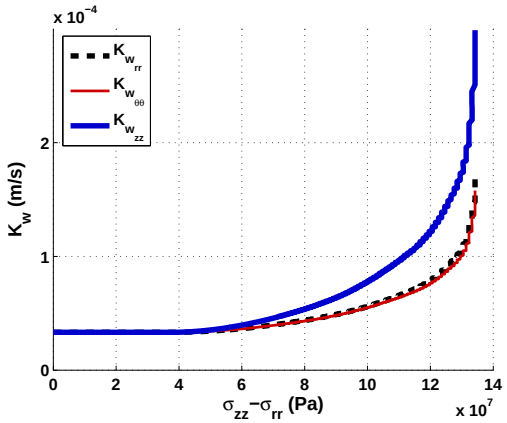

Fig. 6 Evolution of the components of the permeability tensor during the drained triaxial compression test performed on saturated Fontainebleau sandstone, under of confining pressure of 28 MPa.

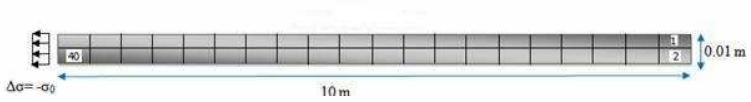

Fig. 7 Adopted mesh for the 1D tunnel problem.

isotropic stress $\boldsymbol{\sigma_0}$, in a one-dimensional axisymmetric configuration (Fig. 7). The mechanical parameter choice is explained in detail in [30]. According to the elastic theory of tunnels, the total stress field evolves as:

$$\begin{cases} \sigma_{rr} = \sigma_0 \left(1 - \frac{R^2}{r^2}\right) \\ \sigma_{\theta\theta} = \sigma_0 \left(1 + \frac{R^2}{r^2}\right) \end{cases} \tag{24}$$

in which R is the radius of the gallery, and r, the radial coordinate. The elastic problem has been solved with the "THHMD" algorithm implemented in Θ-Stock. The numerical results fully agree with the theoretical predictions (Fig. 8), which justifies the use of the program for more complex full-scale studies.

4 Damage trends in a heated unsaturated massif

4.1 Validation in elasticity

The following paragraph is dedicated to the problem of nuclear waste storage presented by Pollock [33] for an unsaturated geological massif. Containers are assumed to be stored in a 100 meter depth horizontal gallery. The ground water is located at 500 meters depth. The tunnel is assumed to be long enough to allow a plane strain analysis. The numerical problem of Pollock [33] is tackled with Θ-Stock by using the mesh presented on Fig. 9. Nuclear waste is modeled by two elements which are considered as heating sources. Heat flows are imposed on both of the element horizontal boundaries.

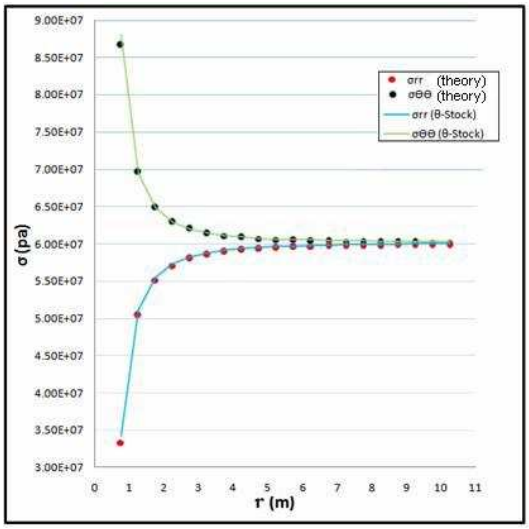

Fig. 8 Comparison of the numerical results to the theoretical predictions in elasticity for the 1D tunnel problem.

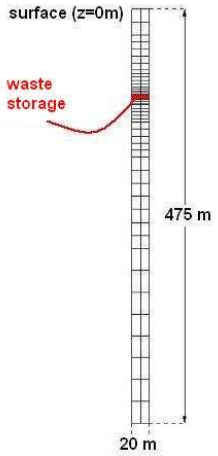

Fig. 9 Adopted mesh for the problem of nuclear waste storage presented by Pollock [33].

Pollock proposed a thermo-hydraulic model dedicated to unsaturated soils. Mechanical aspects are not taken into account in his analysis. On the contrary, simulations performed with Θ-Stock require the use of mechanical degrees of freedom, and thus, the knowledge of the material mechanical parameters. The geological massif has been assumed to have the mechanical behavior of a clay rock, whose parameters have been identified by Homand et al. [24] and by Chiarelli and Shao [8]. The parameters related to fluid and temperature effects are taken from the data given by Pollock [33]. The choice of each parameter is justified in detail in [1]. The most important ones are reported in Tab. 3. The saturation degree is assumed to evolve on a retention

Table 3 Main material parameters used in Pollock nuclear waste storage problem [33].

E	ν	β_s^0	β_T^0	
$1.22 * 10^{10}\, Pa$	0.16	$5.98 * 10^{10}\, Pa$	$5.98 * 10^{10}\, Pa$	
α_{VG}	n_{VG}	k_{w0}	K_{wdg}^{max}	D_{dg}^{max}
$10^{-4}\, Pa^{-1}$	1.361	$5 * 10^{-10}\, m.s^{-1}$	$10^{-9}\, m.s^{-1}$	$10^{-4}\, m^2.s^{-1}$
α_0^*		λ_s	C_{Ps}	
$-7.5 * 10^{-4}\, {}^oC^{-1}$		$1.05\, W.m^{-1}.{}^oC^{-1}$	$837\, J.kg^{-1}.{}^oC^{-1}$	

curve defined by a Van Genuchten model [38], whose parameters are denoted α_{VG} and n_{VG}. D_{dg}^{max} is the vapor conductivity which is assumed to be reached in a 95 percent isotropic damage state. Its value is necessary to compute the internal length parameter b^*, which is involved in the expression of the damaged vapor conductivity (equation 23). α_0^* is the thermal compressibility of the solid skeleton. Its value is negative in the soil mechanics convention. λ_s and C_{Ps} are respectively the thermal conductivity and calorific capacity of the solid skeleton.

The first stage of this study consists in running simulations in the elastic domain in order to check if Θ-Stock program faithfully reproduces the results obtained by Pollock [33]. The damage rigidities to tensile strains are thus equal to zero: $g_M = g_S = g_T = 0$. An initial geothermal temperature gradient is imposed in the massif, the initial surface temperature amounting to $20\, {}^oC$. Fluid pore pressures are initially computed by assuming that the massif is in a hydrostatic state. During the simulation, temperatures and pore pressures are maintained to their initial values at the upper and lower boundaries of the model. Nuclear waste is modeled as a heating source. The heating power initially amounts to $10\, W.m^{-2}$, and then decreases exponentially [33]. Θ-Stock temperature predictions are excellent in the short term as well as in the long term (Fig. 10). The initial saturation state computed by Θ-Stock is some decimals lower than the one which is obtained by Pollock (Fig. 11). The evolution of the saturation degree follow good trends till 100 years of decreasing heating. After 100 years of waste storage, the saturation degree computed by Θ-Stock has an evolution close to the one predicted by Pollock at high depths. Above 90 meters depth, the desaturation zone obtained with Θ-Stock is wider than Pollock's. Surface resaturation (above 20 meters depth) is stronger in the simulations performed with Θ-Stock than in the computations done by Pollock. A better estimate of the retention properties of the geological massif in the "THHMD" model would certainly improve the conformity of the results obtained on the saturation degree to the predictions of Pollock.

4.2 Parametric studies on damage trends

Regarding the difficulty in choosing material parameters, the thermo-hydraulic trends of the "THHMD" program implemented in Θ-Stock are satisfactory in the elastic domain, which justifies the use of the "THHMD" model to predict damage. In the following, two kinds of parametric studies are performed:

1. one damage rigidity (g_S for capillary damage, or g_T for thermal damage) is varied with a fixed maximal damaged permeability K_{wdg}^{max} ;

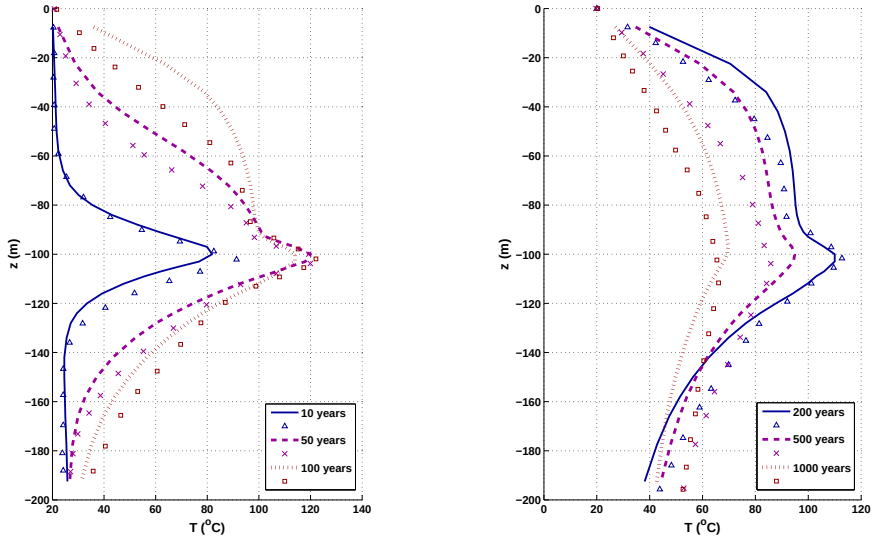

a. b.

Fig. 10 Evolution of temperature in space and time in elasticity. Dots: numerical results from Pollock [33]. Solid lines: numerical results obtained with Θ-Stock.

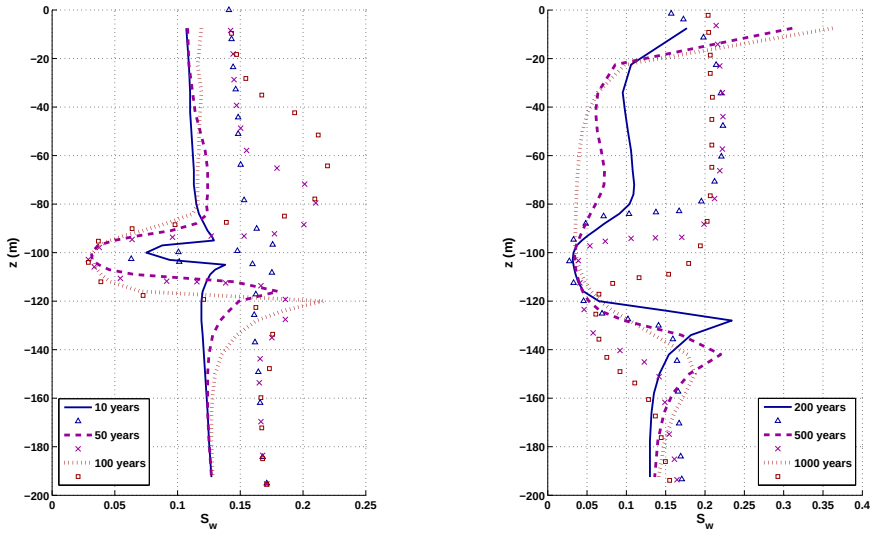

a. b.

Fig. 11 Evolution of the saturation degree in space and time in elasticity. Dots: numerical results from Pollock [33]. Solid lines: numerical results obtained with Θ-Stock.

2. one damage rigidity (g_S or g_T) is fixed to a non-zero value, while the parameter K_{wdg}^{max}, playing the role of an internal length parameter, is varied.

In the following simulations, the maximal damaged vapor conductivity D_{dg}^{max} is assumed to be two orders of magnitude higher than K_{wdg}^{max}. Apart from g_S, g_T, K_{wdg}^{max} and D_{dg}^{max}, all the parameters are identical to the ones used in the elastic study (Tab. 3). The thermal loading is the same as in the preceding elastic simulation, in order to enable comparisons. The values of g_S and g_T are multiples of the value identified by Chiarelli and Shao for clay rock [8]: $g_M^{ref} = -1.414\,Pa$. The presented parametric studies deal with either capillary (g_S) or thermal (g_T) damage, growing with volumetric strains (equation 3). The tensile strains resulting from heating and drying are thus isotropic, which leads to isotropic damage and thus, to an isotropic damaged permeability tensor $\mathbf{K_w}$: $\Omega_{xx} = \Omega_{yy}$, $K_{wxx} = K_{wyy}$. That is the reason why only the horizontal components of damage and permeability are represented in the following.

4.2.1 Damage evolution

Figure 12 shows that damage may develop when $g_T = 0$ if $g_S \neq 0$, which means that due to coupling effects, heating may generate capillary cracking. When a damage rigidity (g_S or g_T) increases, the damaged zone spreads and the intensity of damage grows up. For instance, the damaged zone reaches 200 meters depth after 1000 years of storage for $g_T = 0.004\,g_M^{ref}$. The highest damage values are observed close to the heating source, at 100 meters depth. The peak value is reached in the short term - while the heating power is still high, and generally does not evolve between 50 years and 1000 years of storage. However, the damaged zone spreads in the long term, which testifies the diffusive character of heat transfer. A complete investigation of the numerical results shows that after 200 years, the damaged zone lies between 90 and 110 meters depth for $g_S \neq 0$ and between 40 and 140 meters depth for $g_T \neq 0$. After 1000 years, the damaged zone spreads between 40 and 120 meters depth for $g_S \neq 0$ and between 20 and 200 meters depth for $g_T \neq 0$ (Fig. 12.c,d).
The internal length parameter, computed by means of K_{wdg}^{max} parameter (equation 20), does not influence much the extent of the damaged zone, nor the maximal damage value (Fig. 13). In the long term, capillary damage ($g_S \neq 0$) can reach a slightly higher value for small internal lengths (up to 4 percent more damage for $K_{wdg}^{max} = 10\,k_{w0}$ or $K_{wdg}^{max} = 100\,k_{w0}$ than for $K_{wdg}^{max} = 1000\,k_{w0}$ or $K_{wdg}^{max} = 10000\,k_{w0}$).

4.2.2 Influence of the damage parameters on the liquid water permeability

For a sufficiently high internal length parameter ($K_{wdg}^{max} = 1000\,k_{w0}$), water permeability is significantly affected by damage (equation 19). Liquid water conductivity increases with damage intensity, and, according to the preceding paragraph, with damage rigidities. The results observed on figure 14 confirm this physical statement. For the highest tested damage rigidities, damage peak values amount to up to 12 percent in the vicinity of the heating source (Fig.12). Correspondingly, water permeability is one order of magnitude higher than in the intact state (Fig. 14). The extent of the zone of influence of damage on permeability is larger for thermal damage (up to 200 meters depth for $g_T \neq 0$) than for capillary damage (concentrated around the heating source for $g_S \neq 0$).
According to the model assumptions, the damaged permeability strongly depends on

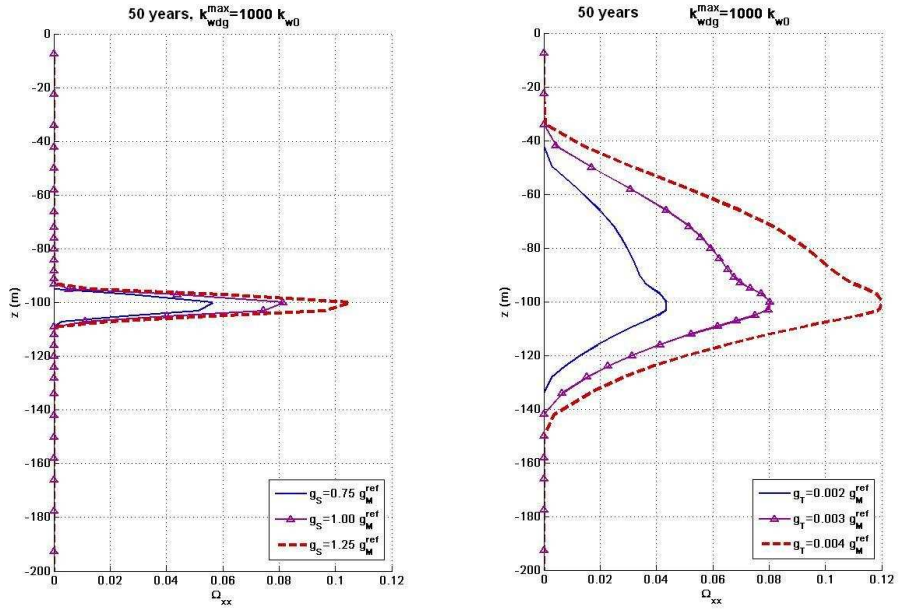

a.

b.

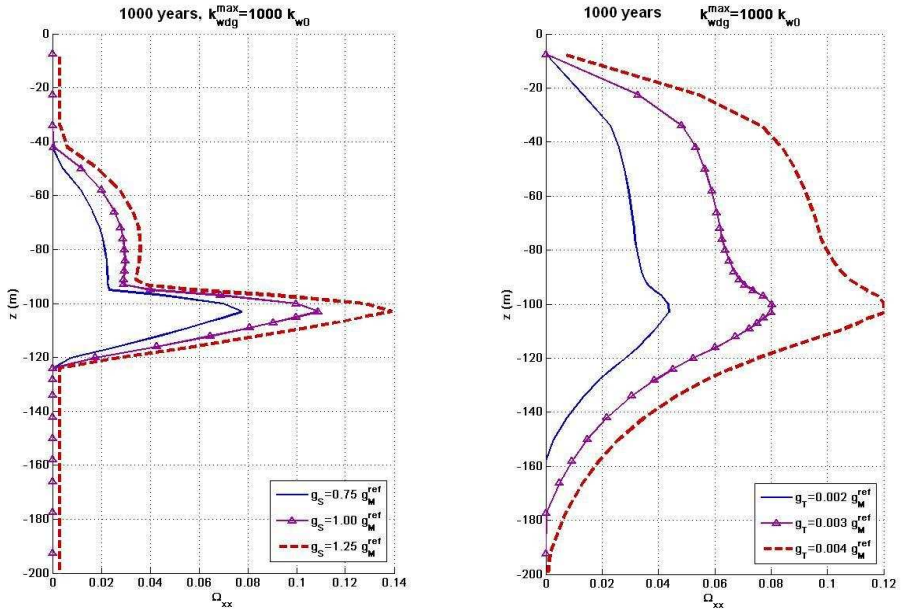

c.

d.

Fig. 12 Influence of damage rigidities on cracking in the problem of nuclear waste storage exposed by Pollock [33]. $K^{max}_{wdg} = 1000\, k_{w0}$. a,c. Influence of g_S. b,d. Influence of g_T.

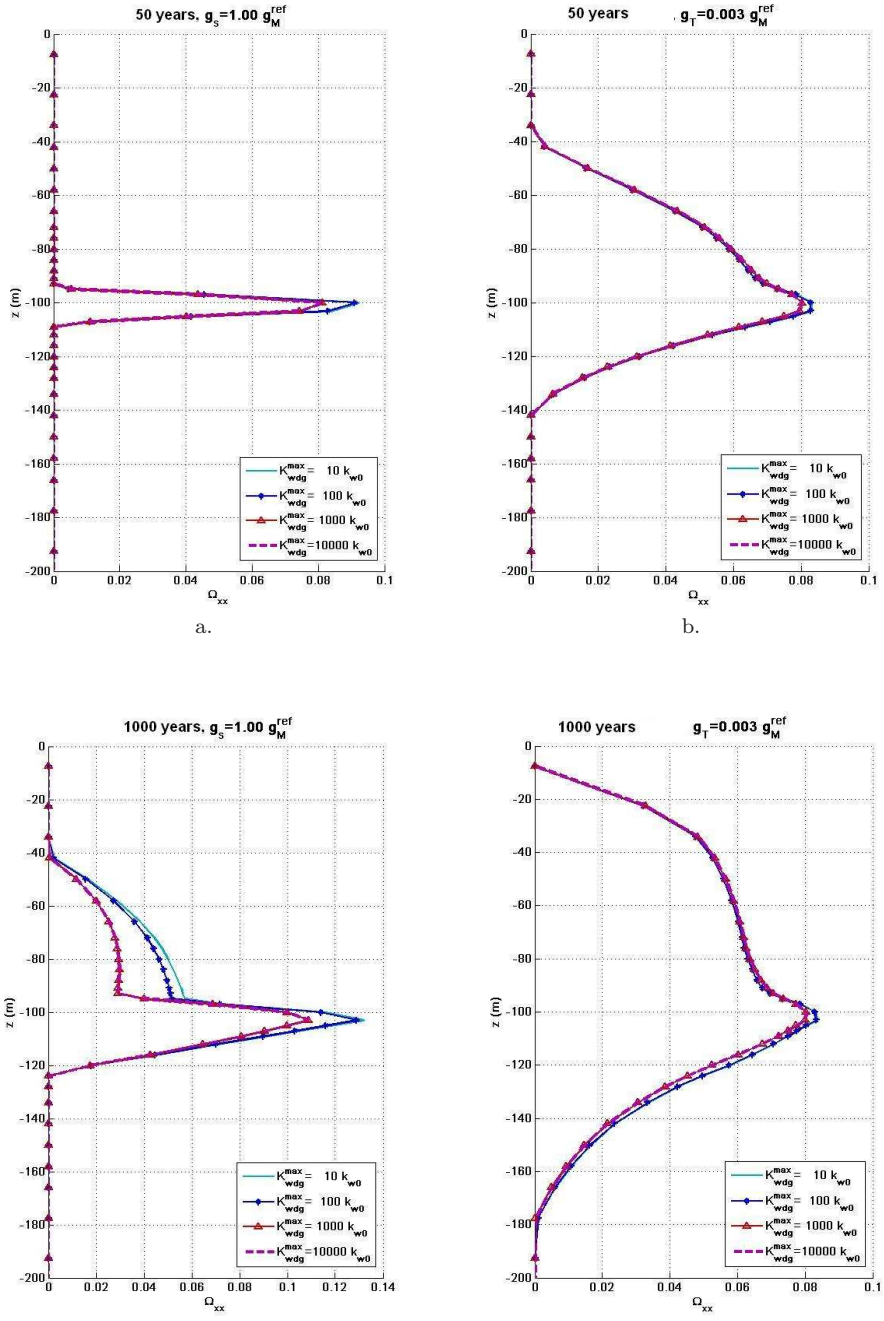

Fig. 13 Influence of the maximal damaged permeability K_{wdg}^{max} on cracking in the problem of nuclear waste storage exposed by Pollock [33]. a,c. $g_S = g_M^{ref}$, $g_T = 0$. b,d. $g_T = 0.003\, g_M^{ref}$, $g_S = 0$.

the internal length parameter (equations 19 and 20). For a given damage rigidity (g_S or g_T), a higher maximal damaged permeability, and thus a higher internal length parameter, results in a higher sensitivity of water conductivity to damage (Fig. 15). For high g_S and g_T values, water permeability increases by up to two orders of magnitude for $K_{wdg}^{max} = 1000\,k_{w0}$ or $K_{wdg}^{max} = 10000\,k_{w0}$. On the contrary, low internal length parameters neutralize damage effects on permeability, as can be seen from the curves obtained for $K_{wdg}^{max} = 10\,k_{w0}$ and $K_{wdg}^{max} = 100\,k_{w0}$. In these latter cases, the additional crack-related permeability $\mathbf{k_2}\,(\mathbf{\Omega})$ is negligible in comparison to the permeability induced by the pores of the intact matrix. The presented parametric studies highlight the important role of the internal length parameter in fluid transfer modeling.

The coupled parametric studies on g_S and g_T on the one hand, and on K_{wdg}^{max} on the other hand, make it possible to assess the dependence of conductivities on damage on the one hand, and to check a possible dependence of damage growth on the increase of permeability on the other hand. Figure 14 shows that damage affects water permeability according to the theoretical assumptions of the "THHMD" model. Figure 13 shows that permeability changes do not contribute to the development of damage.

5 Conclusion

The "THHMD" model is a fully-coupled thermo-hydro-mechanical damage model dedicated to unsaturated porous media. The damage variable is a second-order tensor expressed in its principal base. The model is formulated for a Representative Elementary Volume in net stress, suction and thermal stress independent state variables. The strain tensor is split into three components, each of which being conjugate to a stress state variable (equations 2). Each of the three components encompasses a non-elastic part due to damage growth (equation 3). The increment of damage is computed by an associate flow rule depending on tensile strains. The model development mixes phenomenological and micro-mechanical concepts. On the one hand, the stress/strain relations are derived from a postulated thermodynamic potential. The free energy is assumed to be the sum of damaged elastic deformation energies and of residual strain potentials (equations 12 and 13). On the other hand, the damaged rigidities are computed by applying the Principle of Equivalent Elastic Energy for the three couples of state variables (equations 15 and 16).
Crack-related intrinsic conductivities account for the influence of damage on the orientation and intensity of moisture transfers. Specific internal length parameters are defined to take damage into account in the equations of liquid water flow and vapor flow (equations 19, 20 and 23). Damage is assumed to influence air and heat transfers isotropically, through the inelastic component of volumetric strains, which is involved in the diffusive terms of the flow equations.
The "THHMD" model has been implemented in Θ-Stock Finite Element code [19]. The mechanical aspects of the model have been validated by comparing the numerical results to experimental data and and to theoretical predictions. Isothermal triaxial compression tests performed on saturated geomaterials have also been successfully reproduced in drained and undrained conditions. A full scale study has assessed the ability of the program to predict the behavior of an unsaturated massif hosting a heating source. In the elastic domain, the results given by Θ-Stock are in conformity with the reference temperature and saturation degree evolutions. Moreover, damage and

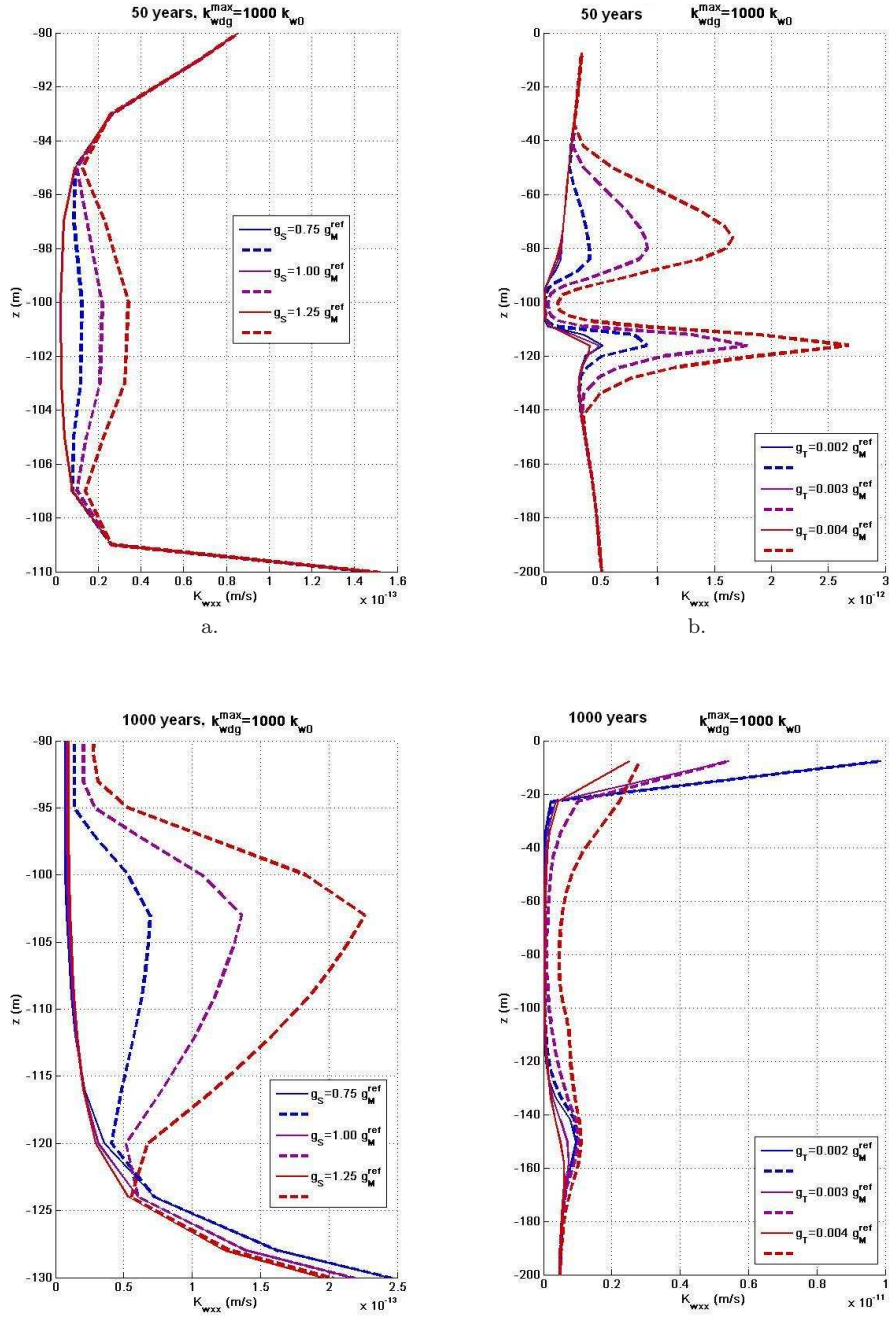

Fig. 14 Influence of damage rigidities on liquid water permeability in the problem of nuclear waste storage exposed by Pollock [33]. $K_{wdg}^{max} = 1000\, k_{w0}$. Solid lines: permeability contribution of the intact porous matrix. Dashed lines: permeability in the damaged material ($K_{wxx} = K_{wyy}$). a,c. Influence of g_S. b,d. Influence of g_T.

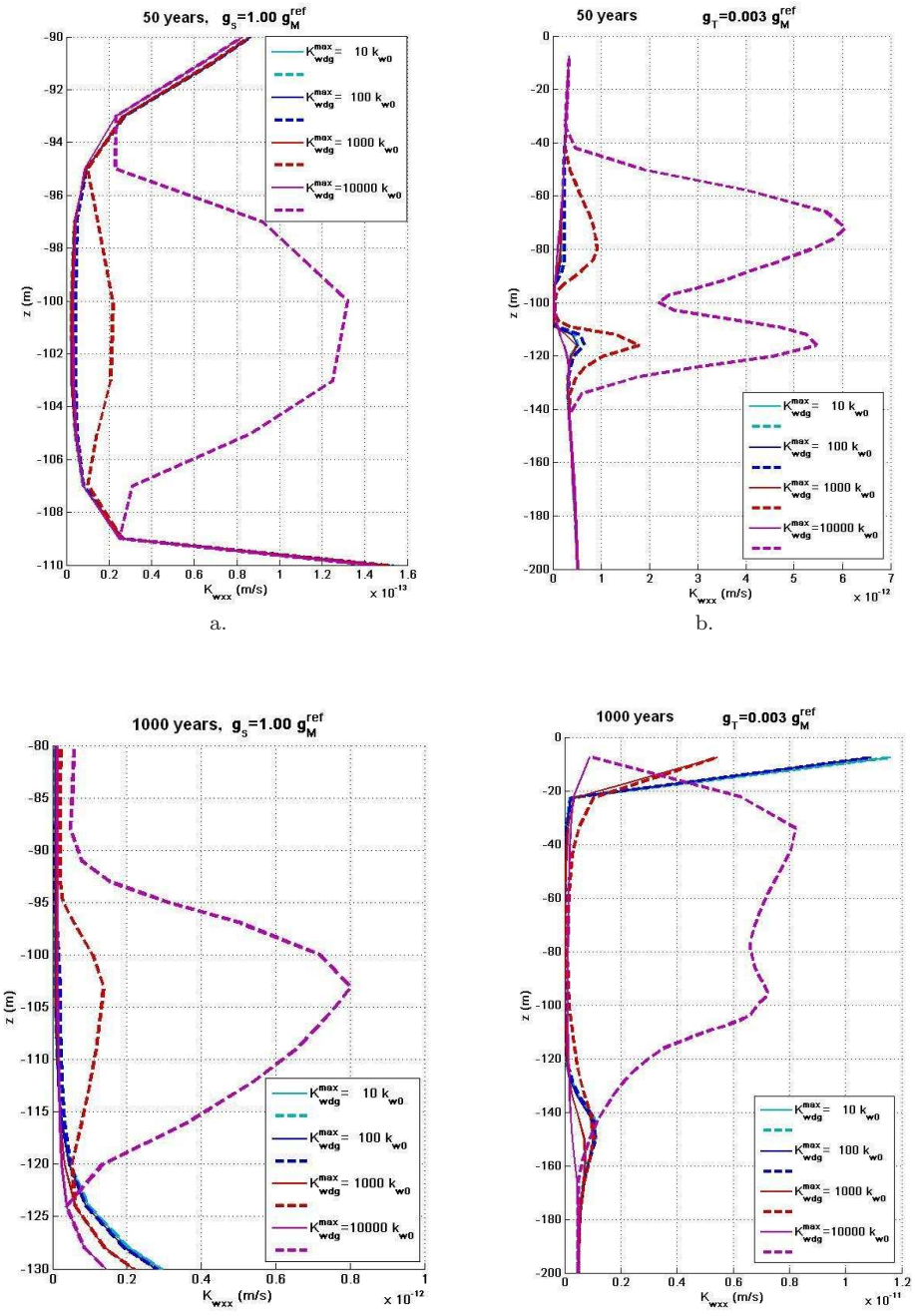

Fig. 15 Influence of the maximal damaged permeability K_{wdg}^{max} on liquid water peremability in the problem of nuclear waste storage exposed by Pollock [33]. Solid lines: permeability contribution of the intact porous matrix. Dashed lines: permeability in the damaged material ($K_{wxx} = K_{wyy}$). a,c. $g_S = g_M^{ref}$, $g_T = 0$. b,d. $g_T = 0.003\, g_M^{ref}$, $g_S = 0$.

permeability trends in the brittle domain are in agreement with the physical assumptions of the "THHMD" model. Additional fully coupled in situ tests are currently being simulated in order to test the model performance. In the mid term, the "THHMD" model is expected to be a useful tool for the design of nuclear waste repositories.

Acknowledgements This research is supported by the European project TIMODAZ (*Thermal Impact on the Damaged Zone Around a Radioactive Waste Disposal in Clay Host Rocks*), launched by EURATOM (*European Community of Atomic Energy*).

References

1. Arson, C.: Etude théorique et numérique de l'endommagement thermo-hydro-mécanique des milieux poreux non saturés. Ph.D. thesis, Ecole Nationale des Ponts et Chaussées, Paris (2009)
2. Arson, C., Gatmiri, B.: Excavation damage in unsaturated porous media. Key Engineering Materials, Advances in Fracture and Damage Mechanics VII **385-387**, 137–140 (2008)
3. Arson, C., Gatmiri, B.: On damage modelling in unsaturated clay rocks. Physics and Chemistry of the Earth **33**, S407–S415 (2008)
4. Arson, C., Gatmiri, B.: A mixed damage model for unsaturated porous media. Comptes-Rendus de l'Académie des Sciences de Paris, section Mécanique **337**, 68–74 (2009)
5. Arson, C., Gatmiri, B.: Parametric study on the performance of a thm damage model for unsaturated porous media. In: Proc. 1st International Symposium on Computational Geomechanics, Juan-les-Pins, France, 29 april - 1er mai 2009, pp. 53–562 (2009)
6. Bazant, Z., Jirasek, M.: Nonlocal integral formulations of plasticity and damage: survey of progress. J. Eng. Mec. ASCE **128**, 1119–1149 (2002)
7. de Borst, R., Pamin, J., Geers, M.: On coupled gradient-dependent plasticity and damage theories with a view to localization analysis. Eur. J. Mech. A/ Solids **18**, 939–962 (1999)
8. Chiarelli, A., Shao, J.: Modélisation élastoplastique couplée à l'endommagement anisotrope pour des argilites. Revue Française de Génie Civil **6**, 115–130 (2002)
9. Collins, I., Houlsby, G.: Application of thermomechanical principles to the modelling of geotechnical materials. Proceedings Mathematical, Physical and Engineering Sciences **453**(1964), 1975–2001 (1997)
10. Cordebois, J., Sidoroff, F.: Endommagement anisotrope en élasticité et plasticité. Journal de Mécanique théorique et appliquée pp. 45–60 (1982)
11. Coussy, O., Dangla, P.: Approche énergétique du comportement des sols non saturés, chap. 4, pp. 137–174. Hermès (2002)
12. Dangla, P., Malinsky, L., Coussy, O.: Plasticity and imbibition-drainage curves for unsaturated soils : a unified approach. Proc. Numerical Models in Geomechanics, Pietruszczak and Pande (eds), Balkema, Rotterdam pp. 141–146 (1997)
13. Dragon, A., Halm, D.: Modélisation de l'endommagement par méso-fissuration : comportement unilatéral et anisotropie induite. C.R. Acad. Sci. Paris **T. 322**(Série IIb), 275–282 (1996)
14. Dragon, A., Halm, D., Désoyer, T.: Anisotropic damage in quasi-brittle solids: modelling, computational issues and applications. Comput. Methods Appl. Mech. Engrg. **183**, 331–352 (2000)
15. Durner, W.: Hydraulic conductivity estimation for soils with heterogeneous pore structure. Water Resources Research **30**(2), 211–223 (1994)
16. Fredlund, D., Morgenstein, N.: Stress state variables for unsaturated soils. J. of the Soil Mechanics and Foundations Division pp. 447–466 (1977)
17. Gatmiri, B.: Framework of a non linear fully coupled thermo-hydro-mechanical behaviour of unsaturated porous media. In: Keynote lecture of the 3rd Iranian International Conference on Geotechnical Engineering and Soil Mechanics. Teheran, Iran (2002)
18. Gatmiri, B.: Non linear behaviour of a multiphase engineering barrier in nuclear waste disposal. In: Proc. 16th ICSMGE, pp. 2261–2264. Osaka, Japan (2005)
19. Gatmiri, B., Arson, C.: Theta-stock, a powerful tool for thermohydromechanical behaviour and damage modelling of unsaturated porous media. Computers and Geotechnics **35**, 890–915 (2008)

20. Gatmiri, B., Seyedi, M., Delage, P., Fry, F.: A new suction-based mathematical model for thermo-hydro-mechanical behavior of unsaturated porous media. In: Proceedings of the 6th International Symposium on Numerical Models in Geomechanics, NUMOG VI, pp. 291–296. Quebec, Canada (1997)
21. Gens, A., Garcia-Molina, A., Olivella, S., Alonso, E., Huertas, F.: Analysis of full-scale in situ test simulating repository conditions. International Journal for Numerical and Analytical Methods in Geomechanics **22**, 515–548 (1998)
22. Halm, D., Dragon, A.: Modélisation de l'endommagement par mésofissuration du granite. Revue Française de Génie Civil **17**, 21–33 (2002)
23. Hansen, N., Schreyer, H.: A thermodynamically consistent framework for theories of elastoplasticity coupled with damage. Int. J. Solids and Structures **31**(3), 359–389 (1994)
24. Homand, F., Chiarelli, A., Hoxha, D.: Caractéristiques physiques et mécaniques du granite de la vienne et de l'argilite de l'est. Revue Française de Génie Civil **6**, 11–20 (2002)
25. Houlsby, G.: The work input to an unsaturated granular material. Gotechnique **47**(1), 193–196 (1997)
26. Kachanov, M.: Effective elastic properties of cracked solids: critical review of some basic concepts. Appl. Mech. Rev. **45** (1992)
27. Lemaître, J., Desmorat, R.: Engineering Damage Mechanics. Ductile, creep, fatigue and brittle failure. Springer - Verlag, Berlin Heidelberg (2005)
28. Martino, J., Chandler, N.: Excavation-induced damage studies at the underground research laboratory. Int. J. Rock Mech. and Min. Sci. **41**, 1413–1426 (2004)
29. Mertens, J., Bastiaens, W., Dehandschutter, B.: Characterization of induced discontinuities in the boom clay around the underground excavations (urf, mol, belgium). Appl. Clay Science **26**, 413–428 (2004)
30. Mozayan, M.: Etude théorique et numérique de d'endommagement en milieu poreux non saturé non isotherme. Master's thesis, Ecole Nationale des Ponts et Chaussées (2009)
31. Philip, J., de Vries, D.: Moisture movement in porous materials under temperature gradients. Transactions, American Geophysical Union **38** (1957)
32. Pires-Domingues, S., Costa-Mattos, H., Rochinha, F.: Modelling of nonlinear damage on elastic brittle materials. Mechanics Research Communications **25** (1998)
33. Pollock, D.: Simulation of fluid flow and energy transport processes associated with high-level radioactive waste disposal in unsaturated alluvium. Water Resources Research **22** (1986)
34. Pruess, K., Wang, J., Tsang, Y.: On thermohydrologic conditions near high-level nuclear wastes emplaced in partially saturated fractured tuff. 2. effective continuum approximation. Water Resour. Res. **26**, 1249–1261 (1990)
35. Shao, J., Zhou, H., Chau, K.: Coupling between anisotropic damage and permeability variation in brittle rocks. International Journal for Numerical and Analytical Methods in Geomechanics **29**, 1231–1247 (2005)
36. Sulem, J., Ouffroukh, H.: Shear banding in drained and undrained triaxial tests on a saturated sandstone: porosity and permeability evolution. International Journal of Rock Mechanics and Mining Sciences **43**, 292–310 (2006)
37. Swoboda, G., Yang, Q.: An energy-based damage model of geomaterials 1. formulation and numerical reults. Int. J. Solids and Struct. **36**, 1719–1734 (1999)
38. VanGenuchten, M.: A closed-form equation for predicting the hydraulic conductivity of unsaturated soils. Soil Science Society of America Journal **44**, 892–898 (1980)
39. Zimmerman, R., Hadgu, T., Bodvarsson, G.: A new lumped-parameter model for flow in unsaturated dual-porosity media. Adv. Water Resour. **19**, 317–327 (1996)